Origin of enhanced magnetization in rare earth doped multiferroic bismuth ferrite

C. Nayek, A. Tamilselvan, Ch. Thirmal, P. Murugavel, and S. Balakumar

Citation: Journal of Applied Physics **115**, 073902 (2014); doi: 10.1063/1.4865958
View online: http://dx.doi.org/10.1063/1.4865958
View Table of Contents: http://scitation.aip.org/content/aip/journal/jap/115/7?ver=pdfcov
Published by the AIP Publishing

Origin of enhanced magnetization in rare earth doped multiferroic bismuth ferrite

C. Nayek,[1] A. Tamilselvan,[2] Ch. Thirmal,[1] P. Murugavel,[1,a)] and S. Balakumar[2]
[1]*Department of Physics, Indian Institute of Technology Madras, Chennai 36, India*
[2]*National Centre for Nanoscience and Nanotechnology, University of Madras, Chennai 25, India*

(Received 5 December 2013; accepted 4 February 2014; published online 20 February 2014)

We report structural and magnetic properties of rare earth doped $Bi_{0.95}R_{0.05}$ FeO_3 (R = Y, Ho, and Er) submicron particles. Rare earth doping enhances the magnetization and the magnetization shows an increasing trend with decreasing dopant ionic radii. In contrast to the x-ray diffraction pattern, we have seen a strong evidence for the presence of rare earth iron garnets $R_3Fe_5O_{12}$ in magnetization measured as a function of temperature, in selected area electron diffraction, and in Raman measurements. Our results emphasised the role of secondary phases in the magnetic property of rare earth doped $BiFeO_3$ compounds along with the structural distortion favoring spin canting by increase in Dzyaloshinskii-Moriya exchange energy. © *2014 AIP Publishing LLC*.
[http://dx.doi.org/10.1063/1.4865958]

I. INTRODUCTION

Multiferroic materials are unique due to the coexistence of ferroelectric, ferroelastic, and ferromagnetic properties with a strong coupling between them.[1,2] They find widespread applications in the field of information storage, spintronics, and sensors.[3,4] Among the multiferroics, $BiFeO_3$ attracted renewed interest due to the existence of ferroic ordering well above room temperature. It shows ferroelectricity up to 1103 K and canted G-type antiferromagnetic ordering at 643 K. The crystal shows weak ferromagnetism due to its symmetry favoring canted antiferromagnetic coupling between (111) planes with resultant non-zero magnetic moment in the unit cell. However, the canted magnetic moment rotates in a spiral direction and forms a spiral spin structure with a period of 62 nm, which cancels out the net magnetization in the bulk.[5,6]

However, efforts are made to improve the magnetic properties of $BiFeO_3$ by substitution of ions from rare earth[7–11] to alkaline earth to transition metals series.[12–15] Several workers have reported the improved magnetic properties in $BiFeO_3$ by rare earth substitution on Bi site and they attribute it to various mechanism. Destruction of the spiral spin arrangement by structural phase transition induced by rare earth ion substitution was thought to be the reason for the enhancement in magnetic properties in La and Nd doped $BiFeO_3$.[7,8] Similarly, the size dependent magnetic properties of $BiFeO_3$ are attributed to the suppression of spiral spin structure.[9] Interestingly, the enhanced magnetization with decrease in particle size upon rare earth doping (Dy^{3+}) is correlated to uncompensated spins at the surface, which leads to incomplete spin compensation between two sublattices.[10] The high remnant magnetization in Eu doped $BiFeO_3$ is attributed to ferromagnetic coupling between the Eu^{3+} and Fe^{3+} ions.[11] On the other hand, it was suggested that the change in Fe-O-Fe bond angle with rare earth substitution may be the reason for the enhanced magnetic moment in rare earth doped (La to Eu) $BiFeO_3$.[16] Although it was reported that the use of gold as crucible made it possible to grow single crystal of $BiFeO_3$ without secondary phases, there are also reports suggesting the presence of impurity phase such as Fe_2O_3, Fe_3O_4, $Bi_2Fe_4O_9$, and $Bi_{25}FeO_{40}$ could contribute to magnetization[17] in doped $BiFeO_3$ [Interestingly, it was demonstrated that the single crystals of $BiFeO_3$ can be grown by flux method without secondary phases using gold crucible[18]]. Alternatively, we found a strong evidence for the presence of $R_3Fe_5O_{12}$ garnets in rare earth doped $BiFeO_3$, which could be the major reason for the reported enhancement in magnetization in doped $BiFeO_3$. In this report, we have carried out the studies on the structural, magnetic, and electrical properties of $Bi_{0.95}R_{0.05}FeO_3$ (R = Y, Ho, and Er), where Ho and Er are magnetic ions and Y is nonmagnetic ion. The results strongly suggest the presence of rare earth iron garnet along with the correlation between the change in character of the Fe-O-Fe bond angle and the magnetization could be the reason for the enhanced magnetization in our sample.

II. EXPERIMENTAL METHODS

The $BiFeO_3$, $Bi_{0.95}Y_{0.05}FeO_3$, $Bi_{0.95}Ho_{0.05}FeO_3$, and $Bi_{0.95}Er_{0.05}FeO_3$ powders are synthesized by sol-gel method. The bismuth acetate, iron acetylacetonate, and rare earth nitrates are used as precursors for Bi, Fe, and rare earth ions, respectively. The relevant amount of precursors are mixed and stirred vigorously for 30 min at 70 °C in a magnetic stirrer till the solution turns yellow in color after homogenous mixing. 2 M citric acid is added to the mixture as gelating agent and the mixture is again stirred for 6 h until the gel formation. The final gel is preheated at 400 °C for 30 min followed by final heat treatment at 800 °C for 2 h. The structural and magnetic properties of the synthesized powder are characterized by x-ray diffraction (XRD) using a PANalytical X'Pert Pro x-ray diffractometer and vibrating sample magnetometer (VSM), respectively. The morphology

a)Author to whom the correspondence should be addressed. Electronic mail: muruga@iitm.ac.in

and particle size of the samples are analyzed using Jeol made Transmission Electron Microscope (TEM).

III. RESULTS AND DISCUSSION

The XRD patterns for pristine, the rare earth doped $BiFeO_3$ are shown in Fig. 1(a) for 2θ ranging from 5° to 70°. All the peaks are indexed to $BiFeO_3$ and we did not see any signature of secondary phases giving the impression that the samples are phase pure. Note that the high intensity (001) peak of $Bi_2Fe_4O_9$ secondary phases appear near the angle 10° is not seen in our pattern. To get the structural information, Reitveld refinement is done on the XRD patterns using GSAS software. As a representative example, the refined data for Y doped $BiFeO_3$ is presented in Fig. 1(b). The refinement shows that the pristine and doped $BiFeO_3$ are crystallized in rhombohedral structure with R3c space group. Among the structural parameters, notably the Fe_1-O-Fe_2 bond angle along [100] direction of the unit cell shows a decreasing trend with decrease in dopant ionic radii. It is 136°, 134.8°, and 133.7° for Y, Ho, and Er doped samples, whose ionic radius is 0.93, 0.89, and 0.88 Å, respectively. The corresponding values for $BiFeO_3$ are 138° and 1.17 Å.

For the morphology and particle size, we have taken the TEM images of the samples and the images are shown in Fig. 2. The particles have arbitrary shape with average particle size of around 300 nm, 250 nm, 120 nm, and 25 nm for the pristine, Y doped, Ho doped, and Er doped $BiFeO_3$. Interestingly, the average size of the particles is decreasing with decrease in dopant ionic radii. The low diffusivity of the rare earth ions, a known grain growth inhibitor, suppresses the grain growth in perovskite.[17] Higher the ionic radii better will be the suppression and lower will be the grain size. However, our samples show opposite trend. Also, the increase in dopant concentration is reported to decrease the particle size by inhibiting the grain growth.[10] But, here the dopant concentration is fixed at 5% for all the samples. Hence, the correlation between the particle size and dopant ionic radii based on the literature is inconclusive and the exact reason is not yet clear.

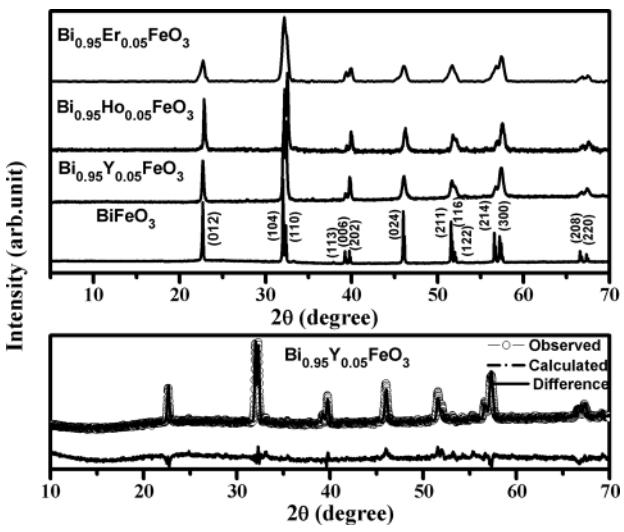

FIG. 1. (a) XRD of pure and rare earth doped $BiFeO_3$ samples. (b) Reitveld refined data for $Bi_{0.95}Y_{0.05}FeO_3$ sample.

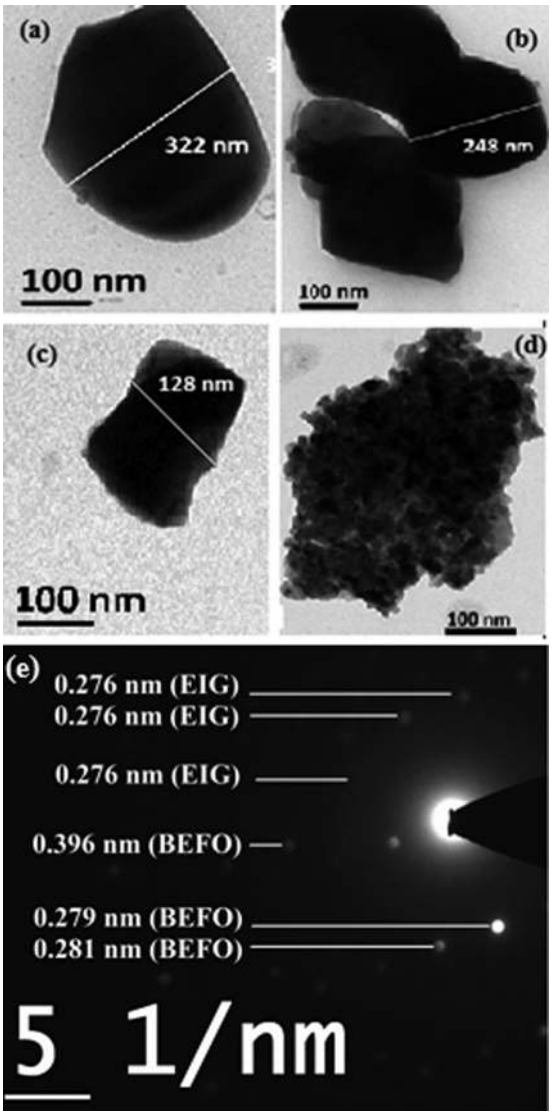

FIG. 2. The TEM images of (a) $BiFeO_3$, (b) $Bi_{0.95}Y_{0.05}FeO_3$, (c) $Bi_{0.95}Ho_{0.05}FeO_3$, and (d) $Bi_{0.95}Er_{0.05}FeO_3$ samples. (e) Selected area electron diffraction pattern of $Bi_{0.95}Er_{0.05}FeO_3$ sample.

To investigate the magnetic properties, we have performed the magnetization versus magnetic field measurement at 300 K and the results are presented in Fig. 3. The parent $BiFeO_3$ shows canted antiferromagnetic signature without significant hysteresis loop opening (see the magnetization data of $BiFeO_3$ presented as inset in Fig. 3) and the magnetization value is 0.067 emu/g at 8 kOe. On the other hand, the rare earth doped samples exhibit higher magnetization as compared to the parent compound. We observed 0.435, 0.57, and 0.612 emu/g as magnetization at 8 kOe for Y, Ho, and Er doped $BiFeO_3$, respectively, which is an increasing trend with decreasing dopant ionic radii. The magnetization observed in our samples is comparable in magnitude with the reported results on doped $BiFeO_3$. In addition, a slender hysteresis loop opening is also observed with the coercive field of 237, 302, and 320 Oe for Y, Ho, and Er doping, respectively. The increase in coercive field is the result of decrease in particle size.

Although the enhancement in magnetization is correlated to the particle size reduction via uncompensated spins

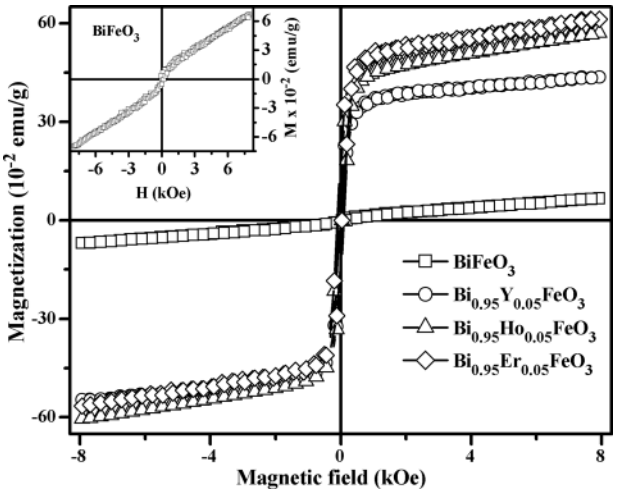

FIG. 3. Magnetization as a function of magnetic field for pure and rare earth doped $BiFeO_3$.

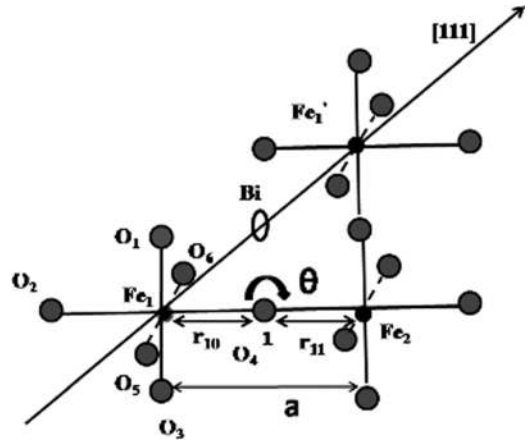

FIG. 4. Schematic diagram showing the structure of $BiFeO_3$. Gray circle and smaller dark circle represent oxygen and Fe ions.

at the surface, the same cannot be said for the magnetic enhancement observed in our samples. Note that the magnetization value for Y and Er doped $BiFeO_3$ samples is 0.435 and 0.612 emu/g, respectively, and the corresponding particle sizes are 250 and 25 nm. Though the Er doped sample shows high magnetization, the fact that the large magnetization observed for Y doped samples, whose particle size is comparable to the parent $BiFeO_3$, precludes the role of particle size alone for the magnetization enhancement. On the other hand, the observed magnetization enhancement in non magnetic Y doped $BiFeO_3$ clearly rules out its origin to be magnetic coupling between the dopant rare earth and Fe^{3+} ions. Alternatively, the change in structural parameters related to the magnetic ion and the surrounding oxygen ligand upon decrease in dopant ionic radii could be correlated to the observed magnetization.

Since the $BiFeO_3$ is a G-type antiferromagnet with its ordering along the [111] direction, the R3c symmetry permits a canting of the antiferromagnetic sublattices resulting a macroscopic weak ferromagnetism.[19] The canting of the Fe^{3+} spins is directly related to antisymmetric Dzyaloshinskii-Moriya exchange energy of Fe^{3+} ion (V_{DM}), which is proportional to $\vec{D}_n \cdot [\hat{s}_0 \times \hat{s}_n]$, where D_n is the Dzyaloshinskii vector given by $\vec{D}_n = V_o(\vec{r}_{n-0} \times \vec{r}_{n-n})$. $\hat{s}_0$ and $\hat{s}_n$ represent the unit vectors along Fe^{3+} magnetic moments. V_o is the microscopic constant, $\vec{r}_{n-0}$ and $\vec{r}_{n-n}$ are the position vectors of the nearest neighbor magnetic ions from the n^{th} oxygen ion (see Fig. 4). As reported,[19] for ideal perovskite structure, the $(\vec{r}_{n-0} \times \vec{r}_{n-n})$ factor is zero and hence the exchange energy term V_{DM} is zero. However, as Fe_1-O-Fe_2 bond angle (θ) start deviating away from ideal 180°, the V_{DM} will increase with an increase in spin canting angle and hence increase in magnetization is expected. In the rare earth doped $BiFeO_3$, the angle θ shows decreasing trend with decrease in dopant ionic radii. The Fe_1-O-Fe_2 bond angle θ is 136°, 134.8°, and 133.7° for Y, Ho, and Er doped $BiFeO_3$ compared to 138° for the pure $BiFeO_3$. Hence, the magnetization enhancement with rare earth in $BiFeO_3$ has strong correlation with the structural distortion induced by dopant substitution, which leads to enhanced Dzyaloshinskii-Moriya exchange energy and hence favoring the spin canting.

To rule out the possible secondary phases contributing to the magnetization from secondary phases, we measured the magnetization as a function of temperature in the high temperature region from 300 K to 700 K. These measurements are largely neglected in the reported literature related to rare earth doped $BiFeO_3$. The results are shown in Fig. 5(a). The pure bismuth ferrite reveals the antiferromagnetic transition with Neel's temperature (T_N) around 643 K, which is matching with the reported bulk value. Interestingly, well below T_N, the magnetization starts increasing down the temperature line indicating the existence of a weak ferromagnetic transition emerging from all the doped samples. The transition is around 590 K, 570 K, and 550 K for Y, Ho, and Er doped sample. For clarity, the derivative of the magnetization versus temperature plot is also shown in Fig. 5(b).

Even if we presume the presence of trace amount of secondary phases like $Bi_{24}Fe_2O_{39}$, $Bi_{25}FeO_{40}$, α-Fe_2O_3, γ-Fe_2O_3, and Fe_3O_4 are present in the sample in a trace amount,

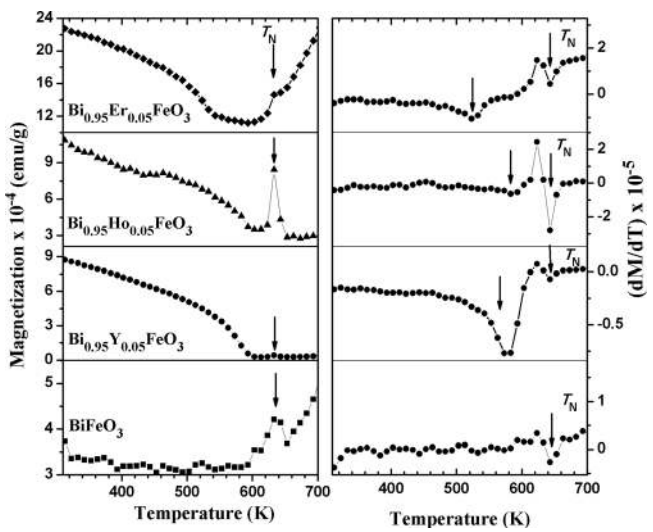

FIG. 5. (a) Magnetization as a function of temperature for pure and rare earth doped $BiFeO_3$ and (b) the derivative of the magnetization versus temperature graph.

which may not be detected by XRD patterns, the observed magnetic transition temperature and its variation with rare earth doping cannot be corroborated with their reported transition temperature for these secondary phases. Remember $Bi_{24}Fe_2O_{39}$ and $Bi_{25}FeO_{40}$ are paramagnetic at room temperature[20,21] and the magnetic transition temperature for α-Fe_2O_3, γ-Fe_2O_3, and Fe_3O_4 nanoparticles is 956 K, 850 K, and 820–986 K well above the observed transition, respectively.[22] However, to our surprise the observed transition is matching well with the ferrimagnetic transition temperatures of $R_3Fe_5O_{12}$ phases. It is 590 K, 570 K, and 560 K for $Y_3Fe_5O_{12}$, $Ho_3Fe_5O_{12}$, and $Er_3Fe_5O_{12}$ garnet.[23–25]

To ascertain it further, we have taken the selected area electron diffraction (SAED) pattern on our sample and as a representative example; the SAED pattern for Er doped BFO is shown in Fig. 2(e). The figure clearly shows the (420) plane (d = 0.276 nm) corresponding to erbium garnet phase (EIG), which is the highest intensity peak of $Er_3Fe_5O_{12}$. The existence of (110), (104), (012) planes of BEFO phase corresponding to the d = 0.279 nm, 0.281 nm, and 0.396 nm, respectively, are also pointed out in Fig. 2(e).

To confirm it further, we have taken the Raman studies on these samples and the spectrum recorded at room temperature is shown in Fig. 6. The figure shows 4 A_1 modes (139 cm^{-1}, 170 cm^{-1}, 207 cm^{-1}, and 433 cm^{-1}) and 9 E modes (124 cm^{-1}, 152 cm^{-1}, 273 cm^{-1}, 333 cm^{-1}, 363 cm^{-1}, 379 cm^{-1}, 471 cm^{-1}, 523 cm^{-1}, and 607 cm^{-1}), which are in agreement with the reported 13 modes for the polycrystalline $BiFeO_3$ samples.[26] Evidence for the $R_3Fe_5O_{12}$ secondary phases could be seen at 474 cm^{-1}, which is the dominant mode for the garnet.[23] Since $BiFeO_3$ also shows E_5 mode at 472 cm^{-1}; for clarity, the derivative version of the Raman plots plotted near these modes are presented as an inset in Fig. 6. The inset shows that the Raman mode for $R_3Fe_5O_{12}$ is seen at 474 cm^{-1} for all samples except the parent compound revealing the proof of its existence. The shift in the higher frequency 472 cm^{-1} mode of BFO after Y, H, and Er doping from 468 cm^{-1} to 472 cm^{-1} can be correlated to the vibration involving rotation of the oxygen octahedral and the resultant structural distortion. The difference in Raman shift observed in the range from 466 to 478 cm^{-1} is intrinsic effect of the compounds rather than the experimental uncertainty. Hence, the presence of $R_3Fe_5O_{12}$ garnet in the rare earth doped compounds is well established by electron diffraction, magnetization vs. temperature, and Raman measurements.

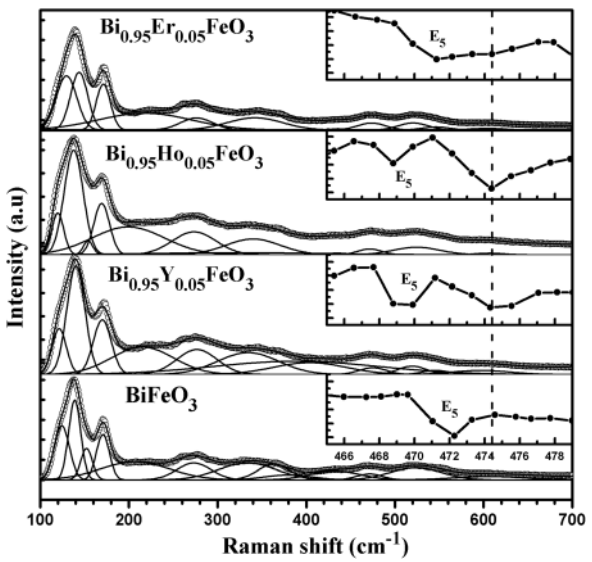

FIG. 6. Raman spectrum recorded for $BiFeO_3$ and $Bi_{0.95}R_{0.05}FeO_3$ (R = Y, Ho, and Er) samples at 300 K. The inset shows its derivative plotted around 470 cm^{-1}.

IV. CONCLUSIONS

$Bi_{0.95}R_{0.05}FeO_3$ submicron particles doped with rare earth ions (R = Y, Ho, and Er) have been prepared by a sol-gel method. Magnetization measured at 300 K revealed enhanced magnetization and shows increasing trend with decrease in ionic radii of the dopant ion. Though the enhanced magnetization can be correlated to the increase in spin canting induced by structural distortion by rare earth substitutions, evidence for the presence of rare earth garnets $R_3Fe_5O_{12}$ is seen from the electron diffraction pattern and magnetization versus temperature graph, where its ferromagnetic transition is clearly revealed. In addition, Raman spectrum also shows a mode corresponding to the $R_3Fe_5O_{12}$ phase confirming its presence in the sample. Hence, we conclude that the major contribution to the enhancement in magnetization could come from the $R_3Fe_5O_{12}$ secondary phase, which is crossly overlooked in the literature due to inadequate magnetic measurements at appropriate temperature range.

[1]G. A. Smolenskii and I. E. Chupis, Sov. Phys. Usp. **25**, 475 (1982).
[2]T. Kimura, T. Goto, H. Shintani, K. Ishizaka, T. Arima, and Y. Tokura, Nature (London) **426**, 55–58 (2003).
[3]M. Fiebig, T. Lottermoser, D. Frohlich, A. V. Goltsev, and R. V. Pisarev, Nature (London) **419**, 818–820 (2002).
[4]J. Wang, J. B. Neaton, H. Zheng, V. Nagarajan, S. B. Ogale, B. Liu, D. Viehland, V. Vaithyanathan, D. G. Schlom, U. V. Waghmare, N. A. Spaldin, K. M. Rabe, M. Wuttig, and R. Ramesh, Science **299**, 1719–1722 (2003).
[5]S. T. Zhang, Y. Zhang, M. H. Lu, C. L. Du, Y. F. Chen, Z. G. Liu, Y. Y. Zhu, N. B. Ming, and X. Q. Pan, Appl. Phys. Lett. **88**, 162901-1–162901-3 (2006).
[6]C. Ederer and N. A. Spaldin, Phys. Rev. B **71**, 224103-1–224103-9 (2005).
[7]P. Suresh and S. Srinath, J. Appl. Phys. **113**, 17D920-1–17D920-3 (2013).
[8]G. L. Yuan, S. W. Or, J. M. Liu, and Z. G. Liu, Appl. Phys. Lett. **89**, 052905-1–052905-3 (2006).
[9]T. J. Park, G. C. Papaefthymiou, A. J. Viescas, A. R. Moodenbaugh, and S. S. Wong, Nano Lett. **7**, 766–772 (2007).
[10]F. Z. Qian, J. S. Jiang, S. Z. Guo, D. M. Jiang, and W. G. Zhang, J. Appl. Phys. **106**, 084312-1–084312-6 (2009).
[11]J. Liu, L. Fang, F. Zheng, S. Ju, and M. Shen, Appl. Phys. Lett. **95**, 022511–022513 (2009).
[12]V. A. Khomchenko, D. A. Kiselev, J. M. Vieira, L. Jian, A. L. Kholkin, A. M. L. Lopes, Y. G. Pogorelov, J. P. Araujo, and M. Maglione, J. Appl. Phys. **103**, 024105-6 (2008).
[13]Y. Wang, J. Li, J. Chen, and Y. Deng, J. Appl. Phys. **113**, 103904-1–103904-5 (2013).
[14]Y. N. Feng, H. C. Wang, Y. D. Luo, Y. Shen, and Y. H. Lin, J. Appl. Phys. **113**, 146101-1–146101-3 (2013).
[15]C. H. Yang, J. Seidel, S. Y. Kim, P. B. Rossen, P. Yu, M. Gajek, Y. H. Chu, L. W. Martin, M. B. Holcomb, Q. He, P. Maksymovych, N. Balke, S. V. Kalinin, A. P. Baddorf, S. R. Basu, M. L. Scullin, and R. Ramesh, Nature Mater. **8**, 485–493 (2009).
[16]S. Vijayanand, H. S. Potdar, and P. A. Joy, Appl. Phys. Lett. **94**, 182507-1–182507-3 (2009).

[17]S. Z. Ma, F. H. Liao, S. X. Li, M. Y. Xu, J. R. Li, S. H. Zhang, S. M. Chen, R. L. Huang, and S. Gao, J. Mater. Chem. **13**, 3096–3102 (2003).
[18]K. Feng, L. C. Wang, J. Lu, Y. Wu, and B.-G. Shen, Cryst. Eng. Commun. **15**, 4900 (2013).
[19]A. K. Zvezdin and A. P. Pyatakov, Eur. Phys. Lett. **99**, 57003-1–57003-5 (2012).
[20]Z. H. Wang, Y. Ding, C. S. Tu, T. C. Lin, Y. D. Yao, and K. T. Wu, IEEE Trans. Mag. **45**, 4341–4344 (2009).
[21]K. Singh, R. K. Kotnala, and M. Singh, Appl. Phys. Lett. **93**, 212902-1–212902-3 (2008).
[22]A. S. Teja and P. Y. Koh, Prog. Cryst. Growth Charact. Mater. **55**, 22–45 (2009).
[23]Y. F. Chen, K. T. Wu, Y. D. Yao, C. H. Peng, K. L. You, and W. S. Tse, Microelectron. Eng. **81**, 329–335 (2005).
[24]V. K. Sankaranarayanan and N. S. Gajbhiye, J. Magn. Magn. Mater. **92**, 217–227 (1990).
[25]A. Maignan, K. Singh, C. Simon, O. I. Lebedev, C. Martin, H. Tan, J. Verbeeck, and G. Van Tendeloo, J. Appl. Phys. **113**, 033905 (2013).
[26]D. Kothari, V. R. Reddy, V. G. Sathe, A. Gupta, A. Banerjee, and A. M. Awasthi, J. Magn. Mater. **320**, 548–552 (2008).